Archives of Biochemistry and Biophysics 516 (2011) 113–120

Contents lists available at SciVerse ScienceDirect

Archives of Biochemistry and Biophysics

journal homepage: www.elsevier.com/locate/yabbi

Steady-state kinetic mechanism of the proline:ubiquinone oxidoreductase activity of proline utilization A (PutA) from *Escherichia coli*

Michael A. Moxley [c], John J. Tanner [a,b], Donald F. Becker [c,*]

[a] Department of Chemistry, University of Missouri-Columbia, Columbia, MO 65211, United States
[b] Department of Biochemistry, University of Missouri-Columbia, Columbia, MO 65211, United States
[c] Department of Biochemistry, University of Nebraska-Lincoln, Lincoln, NE 68588-0664, United States

ARTICLE INFO

Article history:
Received 8 September 2011
and in revised form 14 October 2011
Available online 25 October 2011

Keywords:
PutA
Proline metabolism
Proline:ubiquinone oxidoreductase
Proline dehydrogenase

ABSTRACT

The multifunctional proline utilization A (PutA) flavoenzyme from *Escherichia coli* performs the oxidation of proline to glutamate in two catalytic steps using separate proline dehydrogenase (PRODH) and Δ^1-pyrroline-5-carboxylate (P5C) dehydrogenase domains. In the first reaction, the oxidation of proline is coupled to the reduction of ubiquinone (CoQ) by the PRODH domain, which has a $\beta_8\alpha_8$-barrel structure that is conserved in bacterial and eukaryotic PRODH enzymes. The structural requirements of the benzoquinone moiety were examined by steady-state kinetics using CoQ analogs. PutA displayed activity with all the analogs tested; the highest k_{cat}/K_m was obtained with CoQ_2. The kinetic mechanism of the PRODH reaction was investigated use a variety of steady-state approaches. Initial velocity patterns measured using proline and CoQ_1, combined with dead-end and product inhibition studies, suggested a two-site ping-pong mechanism for PutA. The kinetic parameters for PutA were not strongly influenced by solvent viscosity suggesting that diffusive steps do not significantly limit the overall reaction rate. In summary, the kinetic data reported here, along with analysis of the crystal structure data for the PRODH domain, suggest that the proline:ubiquinone oxidoreductase reaction of PutA occurs via a rapid equilibrium ping-pong mechanism with proline and ubiquinone binding at two distinct sites.

Introduction

The oxidation of proline to glutamate is an energetically important pathway that is shared among prokaryotes and eukaryotes [1]. The first step in the pathway is coupled to reduction of the respiratory chain and is catalyzed by proline dehydrogenase (PRODH),[1] a membrane-associated flavoenzyme, which in eukaryotes is localized in the mitochondria. The importance of proline as a metabolic fuel is well documented in bacteria [2–5], yeast [6], parasites [7], insects [8,9], plants [10] and mammals [4,11,12]. For example, in bacteriods, increased proline oxidative flux is correlated with higher N_2 fixation rates and seed yields [13]. Proline oxidative metabolism has also been shown to be critical for *Helicobacter pylori* colonization of the gut and in the closely related mouse pathogen *Helicobacter hepaticus* [14,15]. In fact, Nagata et al. have shown that patients infected with *H. pylori* have 10-fold higher proline levels than non-infected individuals, and that the pathogen uses L-proline as a preferred respiratory substrate in this biological niche [5].

In Gram-negative bacteria, proline oxidation is catalyzed by PutA, a bifunctional enzyme that combines PRODH and NAD^+-dependent Δ^1-pyrroline-5-carboxylate (P5C) dehydrogenase (P5CDH) domains in the same polypeptide to catalyze the conversion of proline to glutamate (see Scheme 1A) [2,16–18]. In other organisms such as Gram-positive bacteria and eukaryotes, PRODH and P5CDH are separate enzymes.

Structural studies on PutA have shown that the PRODH domain has a core $(\beta\alpha)_8$ barrel structure that noncovalently binds the flavin adenine dinucleotide (FAD) cofactor (Fig. 1A). X-ray crystal structures of the PRODH domain of PutA have shown previously that the proline analog, L-tetrahydro-2-furoic acid (L-THFA), binds to the active site and mimics proline binding [19]. The carboxylate group of L-THFA is coordinated by two active site arginine residues (Arg555 and 556) that help position the proline analog near the *si*-face of flavin (Fig. 1A). The $(\beta\alpha)_8$ barrel core is also found in monfunctional PRODHs from Gram-positive bacteria and is predicted to be the catalytic core in human PRODH [20].

* Corresponding author. Address: Department of Biochemistry, Beadle Center, University of Nebraska, Lincoln, NE 68588-0664, United States. Fax: +1 402 472 472 7842.
E-mail address: dbecker3@unl.edu (D.F. Becker).

[1] *Abbreviations used*: FAD, flavin adenine dinucleotide; *put*, proline utilization; NAD^+, nicotinamide adenine dinucleotide; PRODH, proline dehydrogenase; P5CDH, Δ^1-pyrroline-5-carboxylate dehydrogenase; P5C, Δ^1-pyrroline-5-carboxylate; THFA, tetrahydro-2-furoic acid; DCPIP, dichlorophenolindophenol; EDTA, ethylenediaminetetraacetic acid; MOPS, 3-(*N*-morpholino)-propanesulfonic acid; GSA, γ-glutamate semialdehyde; PCD, protocatechuate dioxygenase; PCA, protocatechuic acid; HEPES, 4-(2-Hydroxyethyl)piperazine-1-ethanesulfonic acid; BCA, bicinchoninic acid; CoQ, ubiquinone; *o*-AB, *o*-aminobenzaldehyde; DBMIB, 2,5-dibromo-3-methyl-6-isopropyl-*p*-benzoquinone.

0003-9861/$ - see front matter © 2011 Elsevier Inc. All rights reserved.
doi:10.1016/j.abb.2011.10.011

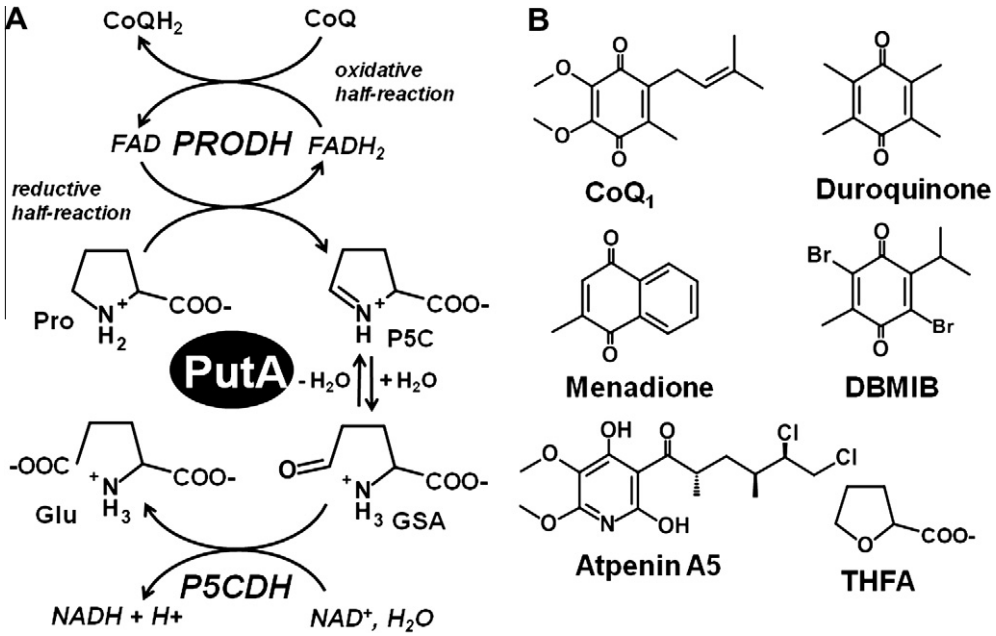

Scheme 1. Overall reaction catalyzed by PutA. (A) (Top) The PRODH domain of PutA catalyzes the proline:ubiquinone oxidoreductase reaction which involves the oxidation of proline and subsequent reduction of CoQ. (Bottom) The P5CDH domain of PutA catalyzes the oxidation of glutamate semialdehyde to glutamate with the concomitant reduction of NAD^+. (B) Chemical structures of CoQ_1, ubiquinone analogs, and THFA.

Typical of flavoenzyme mechanisms, the redox steps catalyzed by the PutA/PRODH domain can be divided into reductive and oxidative half-reactions. In the reductive half-reaction, two electrons from proline are transferred to the flavin cofactor, whereas in the oxidative half-reaction, two electrons are transferred from reduced flavin to an electron acceptor such as ubiquinone (Scheme 1A). After P5C is hydrolyzed to γ-glutamate semialdehyde (GSA), the PutA/P5CDH domain catalyzes the oxidation of γ-GSA to yield glutamate [2,16,17].

In certain Gram-negative bacteria such as *Escherichia coli*, PutA also contains a N-terminal ribbon-helix-helix DNA binding domain that endows PutA with transcriptional regulatory activity [21–23]. The *E. coli* PutA polypeptide has 1320 residues with the DNA-binding, PRODH and P5CDH domains localized at residues 1–52, 261–612, and 650–1130, respectively [1,22]. As a DNA-binding protein, *E. coli* PutA represses transcription of the *putA* and *putP* (Na^+/proline transporter) genes when intracellular proline levels are low [23]. Increases in proline levels induce PutA to bind to the cytoplasmic membrane where it catalyzes the oxidation of proline to glutamate [23]. The mechanism by which PutA switches from a transcriptional repressor to a membrane-bound enzyme relies on proline mediated reduction of the flavin cofactor and subsequent conformational changes that dramatically enhance PutA-membrane interactions [18,24–28].

Although the importance of proline oxidation in bioenergetics is well known, the catalytic mechanism of PutA/PRODH has not been examined in detail. Therefore, we have investigated the PRODH activity in PutA using a variety of steady-state kinetic approaches. This study is the first detailed report on the kinetic mechanism of PutA/PRODH activity and will be helpful for understanding the kinetic properties of other PutAs as well as monofunctional PRODHs.

Materials and methods

Materials

All chemicals and buffers were purchased from Fisher Scientific and Sigma–Aldrich, unless otherwise noted. Atpenin A5 (3-((2S,4S,5R)-5,6-dichloro-2,4-dimethyl-1-oxohexyl)-4-hydroxy-5,6-dimethoxy-2(1H)-pyridinone) was purchased from Enzo life sciences. *E. coli* strains XL-Blue and BL21(DE3) pLysS were purchased from Novagen. Inverted membrane vesicles were prepared from *E. coli* strain JT31 *putA*$^-$ [29]. DL-P5C, which is not commercially available, was synthesized according to the method of Williams and Frank and stored in 1 M HCl at 4 °C [30]. P5C concentrations were determined by measuring the formation of the covalent complex with *o*-aminobenzaldehyde (*o*-AB) at 443 nm (ε_{443nm} = 2590 $M^{-1}cm^{-1}$) [30]. PutA was expressed and purified as previously described [26,27]. PutA was further purified by anion exchange chromatography and eluted from the column (HiTrap Q HP, GE Healthcare) using a 0–1 M NaCl gradient (1 L) in 50 mM Tris (pH 7.5), 0.5 mM EDTA, and 5% glycerol. Purified PutA was dialyzed into 50 mM potassium phosphate buffer (pH 7.4) containing 10% glycerol, 50 mM NaCl, and stored at −80 °C. All experiments used Nanopure water.

Alternative substrate and initial velocity pattern

The concentration of wild-type PutA was determined spectrophotometrically using a molar extinction coefficient of 12,700 $M^{-1}cm^{-1}$ at 451 nm [31]. Steady-state kinetic parameters for duroquinone (tetramethyl-*p*-benzoquinone), menadione (2-methyl-1,4-naphthoquinone), and ubiquinone analogs, CoQ_1, CoQ_2, and CoQ_4 were measured by the decrease in quinone absorbance in the UV range using the following molar extinction coefficients for the quinones: duroquinone (ε_{271nm} = 18.5 $mM^{-1}cm^{-1}$), menadione (ε_{262nm} = 14 $mM^{-1}cm^{-1}$), CoQ_1 (ε_{278nm} = 14.5 $mM^{-1}cm^{-1}$), CoQ_2 (ε_{282nm} = 8 $mM^{-1}cm^{-1}$), and CoQ_4 in 468 μM Triton X-100 (ε_{282nm} = 16.6 $mM^{-1}cm^{-1}$). Assays were performed in 50 mM HEPES (pH 7.4) at 20 °C with 200 mM proline, 0.5 μM PutA enzyme, and varying concentrations of quinone. Triton X-100 (468 μM) was included in assays using CoQ_4. Stock solutions of the quinones were made in ethanol. The final ethanol concentration in the assays was ⩽2%. Assays to obtain steady-state kinetic parameters for proline using different quinones were performed in 50 mM HEPES (pH 7.4) with 0.5 μM PutA, with the product P5C monitored

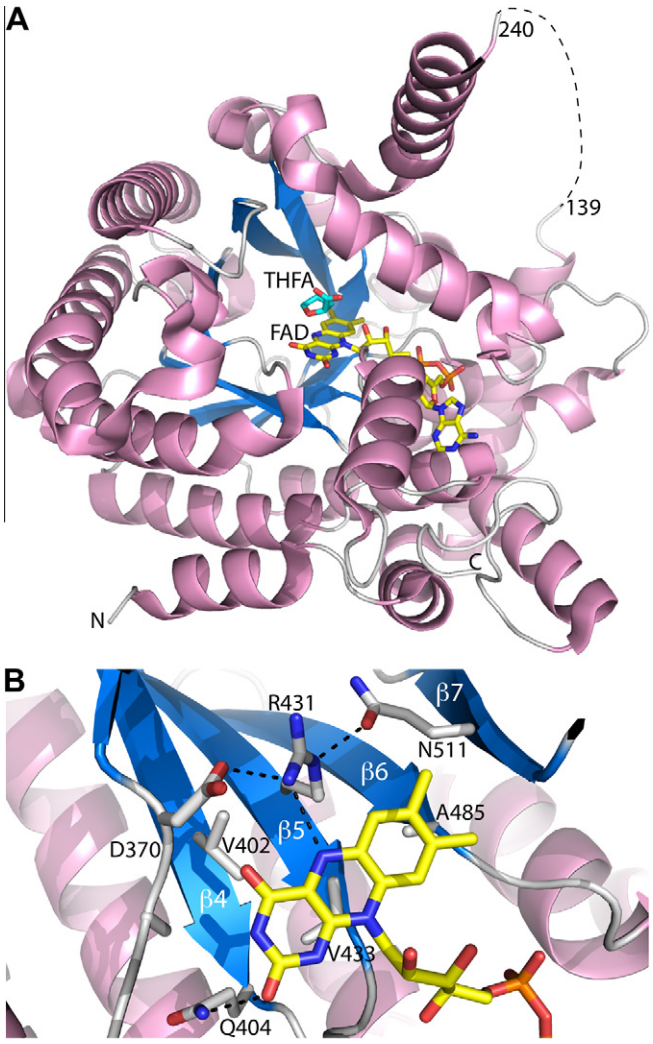

Fig. 1. Structure of the PRODH domain of *E. coli* PutA (PDB 1tiw). (A) The $(\beta\alpha)_8$ barrel core structure of the PRODH domain is shown, highlighting the locations of the FAD cofactor (yellow) and THFA (cyan) bound at the *si*-face of FAD. (B) Illustration of the tight packing of the *re*-face of the FAD cofactor against β strands 4–6 (blue). Figures were generated with PyMOL [55]. (For interpretation of the references to color in this figure legend, the reader is referred to the web version of this article.)

using the *o*-AB reaction [30]. Assays were performed using quinone concentrations at least 3× higher than the respective K_m value for each quinone. Steady-state kinetic parameters for proline obtained with inverted *E. coli* JT31 membrane vesicles were performed in 20 mM MOPS (pH 7.5) containing 10 mM $MgCl_2$, 4 mM *o*-AB, 0.25 μM enzyme and 80 μg/ml of vesicles. The kinetic parameters K_m and k_{cat} were estimated by nonlinear regression analysis of the initial reaction velocity versus proline or quinone concentration using the Michaelis–Menten equation.

To determine the order of substrate binding and product release, steady-state kinetic parameters were determined by varying the proline concentration (5–200 mM) at different fixed amounts of CoQ_1 (15, 25, 50 and 200 μM) and following the decrease in CoQ_1 absorbance at 278 nm. Because a clear ping-pong pattern was observed, the data were fitted globally to the nonlinear form of the ping-pong equation, Eq. (1) [32], in the absence of products (Fig. 2), where v is the initial velocity, $[E]_T$ is the concentration of PutA active sites, k_{cat} is the catalytic constant at infinite $[A]$, $[A]$ and $[B]$ are the concentrations of proline and CoQ_1, respectively, and K_{ma} and K_{mb} are the respective Michaelis–Menten constants for proline and CoQ_1.

$$\frac{v}{[E]_T} = \frac{K_{cat}[A]}{K_{ma} + [A]\left(1 + \frac{K_{mb}}{[B]}\right)} \quad (1)$$

Dead-end inhibition

Dead-end inhibition initial velocity experiments were conducted by varying substrate concentration at different fixed amounts of inhibitor. All assays were performed in 50 mM HEPES (pH 7.4) at 20 °C and followed by the decrease in absorbance at 278 nm from CoQ_1 as above. To determine the type of inhibition and respective inhibition constants, data were fitted globally to the nonlinear forms of the competitive, noncompetitive, uncompetitive, and mixed inhibition equations along with their partial inhibition counterparts using the Enzyme Kinetics Module (1.1) from SYSTAT. Models that were selected to best represent the data are described below.

Initial velocity data with varying amounts of proline (5–200 mM), constant CoQ_1 (200 μM), and different fixed concentrations (0, 2, 6, and 10 mM) of the inhibitor, L-THFA, were fitted to the nonlinear form of the competitive inhibition equation, Eq. (2), where $[S]$ is the varied initial proline concentration, K_m is the Michaelis–Menten constant for proline, $[I]$ is the L-THFA concentration, and K_I is the competitive inhibition constant for L-THFA.

$$\frac{v}{[E]_T} = \frac{K_{cat}[S]}{K_m\left(1 + \frac{[I]}{K_I}\right) + [S]} \quad (2)$$

Initial velocity data with varying amounts of CoQ_1 (5–300 μM), constant proline (100 mM), and different fixed concentrations of L-THFA (0, 0.3, 0.6, 1.2, and 3.0 mM) were fitted to the uncompetitive inhibition model, Eq. (3), where $[S]$ is the initial varied CoQ_1

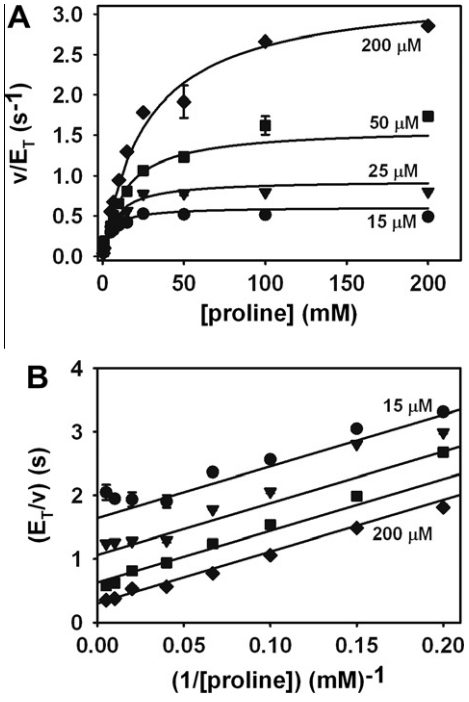

Fig. 2. Initial velocity pattern for PutA with proline as the variable substrate and CoQ_1 as the fixed substrate. (A) Non-linear least squares fit to the ping-pong equation, Eq. (1), with 15 (circles), 25 (triangles), 50 (squares), and 200 μM (diamonds) CoQ_1 and varied proline. The best fit parameters were $k_{cat} = 5.2 \pm 0.3\ s^{-1}$, $K_{ma} = 42 \pm 4$ mM proline, and $K_{mb} = 112 \pm 11$ μM CoQ_1. (B) Double reciprocal plot of the fitted data in panel A with 15, 25, 50 and 200 μM CoQ_1 from top to bottom.

concentration, K_m is the Michaelis–Menten constant for CoQ_1, [I] is the L-THFA concentration and K_I is the uncompetitive inhibition constant [32].

$$\frac{v}{[E]_T} = \frac{K_{cat}[S]}{K_m + [S]\left(1 + \frac{[I]}{K_I}\right)} \quad (3)$$

Initial velocity data with varying amounts of CoQ_1 (5–300 μM), constant proline (100 mM), and different fixed concentrations of Atpenin A5 (0, 20, 100, and 300 μM) were fitted to Eq. (2). Initial velocity data with varying amounts of proline (6.67–200 mM) constant CoQ_1 (110 μM) and fixed concentrations of Atpenin A5 (0, 25, and 300 μM) were fitted to Eq. (3), where [S] is the varied proline concentration, K_m is the Michaelis–Menten constant for proline, [I] is the Atpenin A5 concentration, and K_I is the uncompetitive inhibition constant. Dead-end inhibition data were also analyzed by Hanes–Woolf plots [33].

Product inhibition

Product inhibition studies were conducted by varying substrate concentrations at different fixed concentrations of a single product. All assays were conducted in 50 mM HEPES (pH 7.4) at 20 °C and followed by the decrease in absorbance at 278 nm from CoQ_1 as above. 500 mM NaCl was used to maintain a constant ionic strength throughout the assays. Prior to the assays, DL-P5C stock solutions were neutralized to pH 7.5 with 6 M NaOH. Thus, the addition of neutralized P5C to the assay mixtures increases the NaCl concentration to about 500 mM. The effective concentration of P5C reported for these assays was estimated to be 50% of the DL-P5C concentration since L-P5C is the active stereoisomer. The data were fitted globally to all of the inhibition models mentioned above using the Enzyme Kinetics Module (1.1) from SYSTAT. The best fit models are described below. A product inhibition pattern was obtained by varying proline in fixed concentrations of P5C (0, 1.17, and 3.32 mM) and was best fit to the competitive inhibition model, Eq. (2). CoQ_1 was then varied in fixed P5C (0, 1.17, and 3 mM) and best fit to the uncompetitive inhibition model, Eq. (3). Product inhibition data were also analyzed by Hanes–Woolf plots [33].

Product inhibition by CoQ_1H_2 was tested in assays varying CoQ_1 with fixed proline (30 mM) using a Cary 100 spectrophotometer inside an anaerobic glove box. CoQ_1H_2 was prepared from CoQ_1 by the method of Rieske under anaerobic conditions [34]. The concentration of CoQ_1H_2 was determined by the absorbance at 290 nm with $\varepsilon_{290nm} = 4.14\ mM^{-1}\,cm^{-1}$ [35].

Solvent viscosity effects on steady-state parameters

The effect of solvent viscosity on steady-state kinetic parameters was examined by varying the concentration of proline (0–400 mM) in assays with fixed CoQ_1 (300 μM) and increasing concentrations of D-sucrose (0, 0.65, 1.12, and 1.36 M) in 50 mM Tris (pH 7.5). The solvent viscosity relative to water at 20 °C (η_{rel}) was estimated to be 1, 2, 4, and 6, for assays with 0, 0.65, 1.12, and 1.36 M sucrose, respectively [36]. Data were fitted globally to Eq. (4), where k_{cat} and K_m have their usual meanings, [S] represents the concentration of proline, η_{rel} is the relative viscosity to water mentioned above, m is a factor for the viscosity effect on k_{cat}/K_m, and n is a factor for the viscosity effect on k_{cat} [37]. Initial fitting gave $m = 7.6 \times 10^{-10}$. Thus, data were fitted with $m = 0$ and only n was determined.

$$\frac{v}{[E]_T} = \frac{K_{cat}[S]}{K_m\{1 + m(\eta_{rel} - 1)\} + [S]\{1 + n(\eta_{rel} - 1)\}} \quad (4)$$

PutA tryptophan fluorescence quenching

The binding of the quinone analog, 2,5-dibromo-3-methyl-6-isopropyl-*p*-benzoquinone (DBMIB) (Scheme 1B), to wild-type PutA was examined by intrinsic tryptophan fluorescence quenching of PutA. PutA (1 μM, 0.6 ml volume) in 50 mM potassium phosphate (pH 7.5) was excited at 295 nm while the fluorescence emission spectrum between 300 and 500 nm was collected using a Varian Eclipse spectrofluorometer. The PutA solution was titrated with increasing concentrations of DBMIB (0–20 μM) and the decrease in the fluorescence emission maximum of PutA at 338 nm was monitored. The observed fluorescence at 338 nm was corrected for the inner filter effect caused by the absorption of incident light by DBMIB at 295 nm using Eq. (5) [38]. In eq. (5), F_{corr} and F_{obs} are the corrected and observed fluorescence intensities, respectively, and A_{ex} and A_{em} are the respective absorbance values of DBMIB at the excitation (295 nm) and emission (338 nm) wavelengths.

$$F_{corr} = F_{obs}10^{\left(\frac{A_{ex}+A_{em}}{2}\right)} \quad (5)$$

An equilibrium dissociation constant (K_d) for the PutA–DBMIB complex was determined by fitting the changes in fluorescence to Eq. (6), where θ is the fraction of DBMIB bound and n is the number of binding sites.

$$\theta = \frac{n[DBMIB]_{free}}{K_d + [DBMIB]_{free}} \quad (6)$$

The concentration of free DBMIB ($[DBMIB]_{free}$) was calculated by Eq. (7).

$$[DBMIB]_{free} = [DBMIB]_{total} - \theta[PutA]_{total} \quad (7)$$

θ was determined by $(F_0 - F)/(F_0 - F_{max})$, where F_0, F, and F_{max} are the fluorescence intensities in the absence, presence, and extrapolated infinite amount of DBMIB, respectively. F_{max} was determined by fitting the normalized fluorescence intensity to a general hyperbolic equation.

Incubation of PutA with CoQ_2 and CoQ_1H_2

PutA (60 μM) in 50 mM potassium phosphate buffer (pH 7.4, 50 mM NaCl, and 10% glycerol) was incubated with increasing amounts of CoQ_2 up to a final concentration of 50 μM CoQ_2. The spectrum of the final PutA (60 μM)-CoQ_2 (50 μM) mixture was recorded on a Cary 100 spectrophotometer (300–700 nm). To subtract the spectrum of CoQ_2, a 50 μM CoQ_2 solution without PutA was used to baseline the instrument. To test PutA activity with CoQ_1H_2, oxidized PutA (20 μM after mixing) was degassed and mixed with 260 μM of CoQ_1H_2 under anaerobic conditions in the glove box. After mixing, changes in absorbance of the FAD cofactor were monitored (300–700 nm) for 45 min using a Cary 100 spectrophotometer in the glove box and spectral kinetics software.

Table 1
Kinetic parameters for ubiquinone analogs.[a]

Analog	K_m (μM)	k_{cat} (s^{-1})	k_{cat}/K_m ($M^{-1}s^{-1}$)
Duroquinone	147 ± 27	1.2 ± 0.1	8400 ± 1700
Menadione	79 ± 5	3.5 ± 0.1	44,000 ± 3100
CoQ_1	110 ± 15	3.4 ± 0.2	31,000 ± 4600
CoQ_2	16 ± 4	1.4 ± 0.1	87,000 ± 23,000
CoQ_4	34 ± 4	0.22 ± 0.04	6700 ± 1400

[a] Assays were performed using 200 mM proline.

Table 2
Kinetic parameters for proline with different electron acceptors.[a]

Analog	K_m (mM)	k_{cat} (s^{-1})	k_{cat}/K_m ($M^{-1}s^{-1}$)
Duroquinone	27 ± 2	1.00 ± 0.02	37 ± 2.8
Menadione	67 ± 6	2.4 ± 0.1	36 ± 3.6
CoQ_1	47.5 ± 2.5	3.30 ± 0.05	70 ± 3.8
CoQ_2	9.6 ± 1.3	1.10 ± 0.03	115 ± 16
CoQ_4	2.3 ± 0.5	0.20 ± 0.01	87 ± 19
Membrane vesicles	1.5 ± 0.3	0.43 ± 0.02	287 ± 59

[a] Parameters were estimated from assays which follow *o*-AB-P5C complex formation.

Table 3
Kinetic parameters for dead-end and product (P5C) inhibition.

Inhibitor	Variable substrate	Type of inhibition	K_I
THFA	Proline	Competitive	1.6 ± 0.1 mM
THFA	CoQ_1	Uncompetitive	0.39 ± 0.02 mM
Atpenin A5	Proline	Uncompetitive	124 ± 8 μM
Atpenin A5	CoQ_1	Competitive	97 ± 8 μM
P5C	Proline	Competitive	0.64 ± 0.04 mM
P5C	CoQ_1	Uncompetitive	1.0 ± 0.07 mM

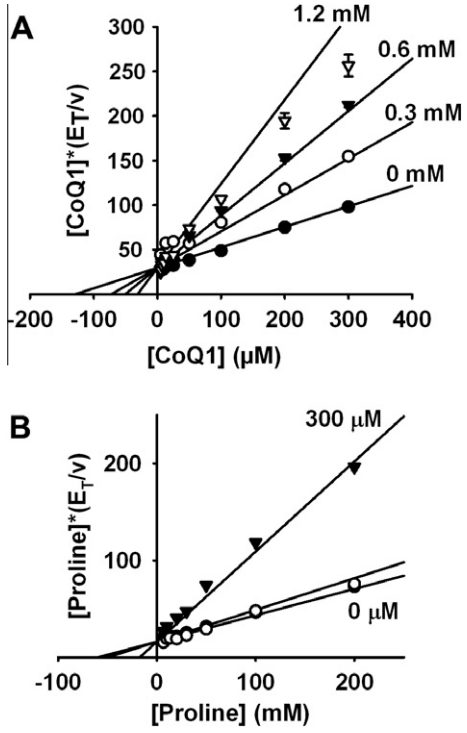

Fig. 3. Dead-end inhibition initial velocity patterns for PutA. (A) Uncompetitive inhibition of PutA by THFA versus CoQ_1. Non-linear least squares fit to the uncompetitive inhibition equation, Eq. (3), displayed as a Hanes–Woolf plot with 0 (circles), 0.3 (open circles), 0.6 (inverted triangles), and 1.2 mM (open inverted triangles) L-THFA and varied CoQ_1. The best fit parameters were K_m = 130 ± 8 μM CoQ_1, k_{cat} = 4.4 ± 0.1 s^{-1}, K_I = 0.39 ± 0.02 mM. (B) Uncompetitive inhibition of PutA by Atpenin A5 versus proline. A non-linear least squares fit to Eq. (3) displayed as a Hanes–Woolf plot with 0 (open circles), 25 (closed circles), and 300 μM (inverted triangles) Atpenin A5 and varied proline. Best fit parameters are k_{cat} = 3.7 ± 0.1 s^{-1}, K_m = 60 ± 3 mM proline, and K_I = 124 ± 8 μM Atpenin A5.

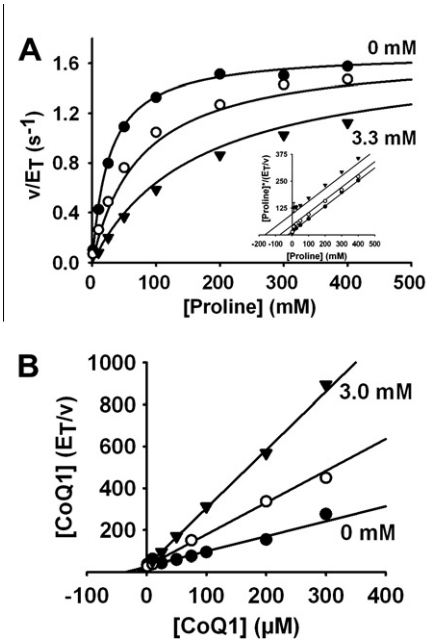

Fig. 4. Product inhibition pattern with P5C. (A) A non-linear least squares fit to the competitive inhibition equation, Eq. (2), with 0 (circles), 1.17 (open circles), 3.3 mM (inverted triangles) P5C and varied proline. Best fit parameters were k_{cat} = 1.70 ± 0.02 s^{-1}, K_m = 26.6 ± 1.4 mM proline, and K_I = 0.64 ± 0.04 mM P5C. (Inset) Hanes–Woolf replot of the data shows a parallel line pattern indicating P5C is competitive with proline. (B) A non-linear least squares fit to the uncompetitive inhibition equation, Eq. (3), displayed as a Hanes–Woolf plot with 0 (circles), 1.17 (open circles), and 3 mM (inverted triangles) P5C and varied CoQ_1. The best fit parameters were k_{cat} = 1.40 ± 0.04 s^{-1}, K_m = 36.7 ± 3.3 μM CoQ_1, and K_I = 1.0 ± 0.07 mM P5C. Note that these assays contained approximately 500 mM NaCl which diminished k_{cat}.

Results

Alternative substrates and initial velocity pattern

The kinetic parameters K_m and k_{cat} for PutA with different ubiquinone analogs were determined using a saturating concentration of proline. Table 1 shows k_{cat} values in the range 0.2–3.5 s^{-1} with the lowest activity observed with CoQ_4. The highest catalytic efficiency (k_{cat}/K_m) was observed with menadione and CoQ_2. These results indicate that although the isoprene side chain is not essential for PutA reactivity with quinones, it does influence the catalytic efficiency of PutA. Table 2 shows that the k_{cat}/K_m for proline with different electron acceptors under saturating conditions varies from 36 $M^{-1}s^{-1}$ with menadione to 287 $M^{-1}s^{-1}$ using membrane vesicles.

The steady-state reaction mechanism of PutA was investigated by performing assays in which CoQ_1 (15–200 μM) and proline (5–200 mM) concentrations were varied. Fig. 2 shows that the data fit well to the ping-pong mechanism, Eq. (1). The kinetic parameters were estimated by fitting the data to a ping-pong mechanism with k_{cat} of 5.2 s^{-1} and K_m values of 42 mM and 112 μM for proline and CoQ_1, respectively. Slight substrate inhibition by proline was observed in assays using low CoQ_1 (15 μM) and high proline concentration (200 mM).

Dead-end and product inhibition experiments

Dead-end inhibition studies were performed to rule out an obligatory ternary mechanism. The inhibition of PutA was first evaluated with L-THFA, an isostructural analog of proline (see Scheme 1B).

The type of inhibition and K_I values for L-THFA versus proline and CoQ_1 are listed in Table 3. L-THFA is a competitive inhibitor of PutA with respect to proline (Fig. S1A). When varying CoQ_1, L-THFA shows inhibition of PutA that is best fit by an equation for uncompetitive inhibition (Fig. 3A).

Inhibition of PutA with the ubiquinone analog, Atpenin A5 [39], was examined by varying proline and CoQ_1 (see Scheme 1B). Aptenin A5 is competitive versus CoQ_1 with $K_I = 97$ μM (Table 3 and Fig. S1B). With respect to proline, Atpenin A5 exhibited uncompetitive inhibition of PutA (Table 3 and Fig. 3B). The results from the steady-state dead-end inhibition profiles using L-THFA and Atpenin A5 are consistent with a ping-pong mechanism [40].

Product inhibition studies were next performed to help distinguish between one- and two-site ping pong mechanisms. Dead-end inhibition patterns for one-site and two-site ping pong mechanisms are identical so they cannot distinguish between these two mechanisms [40]. Product inhibition, however, exhibits opposite patterns [40]. The inhibition of PutA with the products, P5C and CoQ_1H_2, was studied under conditions in which proline or CoQ_1 was varied. The inhibition patterns of P5C versus proline and P5C versus CoQ_1 were best fit to competitive and uncompetitive inhibition models, respectively (Table 3 and Fig. 4). The product inhibition pattern with P5C is suggestive of a two-site ping-pong mechanism.

The effect of CoQ_1H_2 on PRODH activity was next examined but inhibition was not observed with up to 800 μM CoQ_1H_2. CoQ_1H_2 (260 μM) was also incubated with PutA (20 μM) under anaerobic conditions with the FAD spectrum of oxidized PutA monitored for possible reduction by CoQ_1H_2. After 45 min of incubation, reduction of the FAD cofactor by CoQ_1H_2 was not apparent (Fig. S2).

Viscosity dependence of the steady-state parameters

To explore whether diffusive steps are rate limiting during turnover, the effect of viscosity on k_{cat}/K_m and k_{cat} was analyzed by performing steady-state assays in the presence of increasing amounts of the viscogen, D-sucrose [37,41]. D-Sucrose was added to the assay buffer to generate viscosities relative to water (η_{rel}, 20 °C) of 1, 2, 4, and 6. Fig. 5A shows the effect of viscosity on k_{cat} by fitting the steady-state kinetic parameters to Eq. (4). Fitting the data globally to Eq. (4) gave $n = 0.15 \pm 0.02$, indicating that increasing viscosity in the medium decreases k_{cat} by 15% of its initial value when η_{rel} increases by one unit. The change in k_{cat} as a function of η_{rel} was also evaluated by plotting the ratio of $(k_{cat})^0/(k_{cat})$ against η_{rel} (20 °C), where $(k_{cat})^0$ and (k_{cat}) are the catalytic constants determined in the absence and presence of viscogen, respectively (Fig. 5B). If k_{cat} is 100% diffusion limited, the slope of this plot will be unity; otherwise, the slope will be <1. The slope of the plot of $(k_{cat})^0/(k_{cat})$ versus η_{rel} is 0.2 indicating a small decrease in k_{cat} with increased viscosity of the solution. From these results, it appears a product diffusion step limits k_{cat} by about 20%.

Spectroscopic analysis of quinone binding

The binding of quinone to PutA was studied by fluorescence quenching using the brominated quinone analog, DBMIB, which PutA can utilize as an alternate substrate ($k_{cat} \sim 4\ s^{-1}$). Previous studies have shown that DBMIB is superior to CoQ in quenching protein tryptophan fluorescence, thus, making it a useful analog for monitoring quinone-protein binding [42]. DBMIB caused quenching of PutA tryptophan fluorescence at 338 nm in a saturating manner, from which a K_d of 5.7 ± 0.5 μM ($n = 0.88 \pm 0.03$) for the DBMIB–PutA complex was estimated (Fig. 6).

To gain insight into the spatial relationship between quinone and proline binding sites, the DBMIB test was repeated in the presence of THFA. As described above, THFA is a competitive inhibitor with respect to proline and as shown in Fig. 1A, THFA is known to occupy the proline binding site [19]. Thus, if proline and quinone have overlapping binding sites, one expects the K_d for DBMIB to increase in the presence of THFA. The K_d value for DBMIB binding to PutA in the presence of 200 mM THFA is 4.9 ± 0.4 μM ($n = 0.83 \pm 0.03$), which is nearly identical to the value obtained in the absence of THFA. This result is consistent with proline and ubiquinone having separate binding sites.

Given that substrate binding to flavoproteins often perturbs the flavin spectrum, oxidized PutA was titrated with CoQ_2 [43]. The flavin spectrum was unperturbed, suggesting that CoQ_2 does not significantly influence the flavin active site environment (Fig. S3). Addition of DBMIB to PutA also did not perturb the flavin spectrum. Because DBMIB is an alternate substrate and is shown to bind PutA by tryptophan fluorescence (Fig. 6), the lack of changes in the flavin spectrum with CoQ_2 or DBMIB is not due to the absence of binding, but rather suggests that the ubiquinone binding site is located at a position that is too distant from the isoalloxazine ring to significantly alter the flavin spectrum.

Discussion

The k_{cat}/K_m values for the ubiquinone analogs varied by 10-fold with the lowest and highest values determined for CoQ_4 and CoQ_2, respectively. The k_{cat} values were similar with all the ubiquinone analogs tested, with CoQ_4 being the exception. The physiological ubiquinone substrate in the *E. coli* cytoplasmic membrane has 8 isoprene units (CoQ_8). Thus, it is somewhat surprising that CoQ_4 appears to be the least efficient substrate. However, the presence of a membrane or a detergent micelle could considerably affect the outcome of such studies [44]. Interestingly, PutA is able to utilize duroquinone indicating that the isoprene side chain is not essential for PutA reactivity with quinones. Other studies have drawn similar conclusions with the efficacy of the isoprene side chain length [42,45]. Slight substrate inhibition was observed

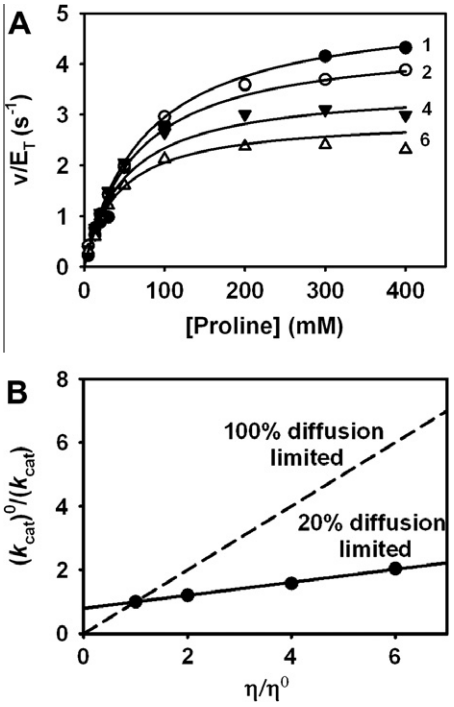

Fig. 5. Effect of increasing solvent viscosity on steady-state kinetics. (A) Non-linear least squares fit to Eq. (4) with 0, 0.65, 1.12, 1.36 M D-sucrose which corresponds to a viscosity relative to water at 20 °C (η_{rel}) of 1, 2, 4, and 6 in varied proline concentrations [35]. (B) The ratio $(k_{cat})^0/(k_{cat})$ was plotted against η_{rel}, where $(k_{cat})^0$ is the catalytic constant in the absence of viscogen, (k_{cat}) is the catalytic constant in the presence of viscogen, and η/η^0 is the relative viscosity to water at 20 °C. The data were fitted to a line to yield a slope value of $0.2 \pm (5 \times 10^{-3})$ for which slope = $\Delta\{(k_{cat})^0/(k_{cat})\}/\Delta(\eta_{rel})$.

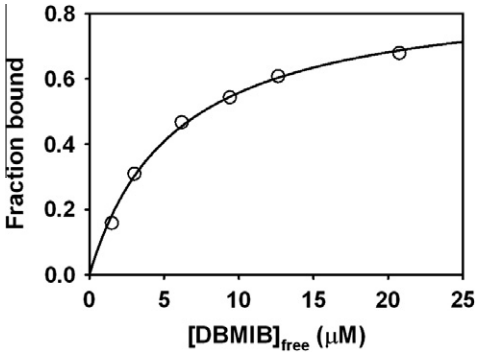

Fig. 6. Tryptophan fluorescence quenching of PutA with DBMIB. One micro molar solution of PutA was titrated with DBMIB while monitoring tryptophan fluorescence (ex. 295 nm, em. 338 nm). Data were fitted to Eq. (6). Inner filter effects caused by DBMIB were corrected as discussed in materials and methods.

(Fig. 2) under reaction conditions of proline $\gg K_m$ and $CoQ_1 \ll K_m$; it is possible that proline may bind weakly to the ubiquinone site, thereby interfering with CoQ_1 binding. Proline may also bind to an alternative form of the enzyme (e.g., reduced form) under the assay conditions resulting in the formation of an enzyme complex that is not competent in catalysis. Other enzymes that adhere to a two-site ping pong mechanism have displayed more severe competitive substrate inhibition including the original mechanism by Northrop [46].

Our kinetic data with *E. coli* PutA show evidence for a two-site ping-pong mechanism for the proline:ubiquinone oxidoreductase reaction. A previous study with PutA from *Salmonella typhimurium* indicated a ping pong mechanism as well [17], however, dead-end and product inhibition studies were not conducted, which are necessary for proper conclusions to be drawn as ternary mechanisms can still produce parallel lines on a Linweaver–Burk plot [32]. Furthermore, product inhibition studies are required to further distinguish between one-site and two-site ping-pong mechanisms [40]. Our results with the dead-end inhibitors show THFA is competitive with respect to proline as expected from the X-ray structure of the PRODH domain (Fig. 1A), and uncompetitive with respect to CoQ_1, whereas Atpenin A5 is competitive with respect to CoQ_1 and uncompetitive with respect to proline. Recent structural studies have shown that Atpenin A5 is a specific ubiquinone binding site inhibitor of succinate:ubiquinone oxidoreductase in *E. coli* [39]. Product inhibition with P5C gave a competitive and uncompetitive pattern versus proline and CoQ_1, respectively. This product inhibition pattern is predicted for a two-site ping-pong rapid equilibrium mechanism. Mixed inhibition (or non-competitive), however, is also possible. The mechanistic difference originates from the reversibility of the reductive half-reaction between the substrate proline and the product, P5C. The uncompetitive inhibition observed with P5C versus CoQ_1 indicates that P5C does not significantly oxidize $FADH_2$ under steady-state conditions. The inability to detect product inhibition with CoQ_1H_2, indicates that the K_I for CoQ_1H_2 is high with respect to the concentration range normally used for CoQ_1. Uncompetitive patterns were also obtained for nitrate reductase and dihyroorotate dehydrogenase which have been proposed to follow a two-site ping-pong rapid equilibrium mechanism [47,48]. Altogether, dead-end and product inhibition patterns observed with PutA are consistent with a two-site ping-pong mechanism with the FAD cofactor in PutA transferring electrons between the proline binding site and a second ubiquinone binding site.

A two-site ping-pong mechanism is not uncommon for oxidoreductase reactions [49]. Physiologically, two binding sites in PutA seem necessary as proline, a soluble substrate, and ubiquinone, a hydrophobic substrate embedded in the membrane, require simultaneous access to the FAD when PutA is bound to the *E. coli* cytoplasmic membrane [50]. In PutA, both faces of the FAD cofactor appear to be occupied with proline binding on the *si*-face of the FAD and the *re*-face of the isoalloxazine ring tightly packed against β strands 4–6 of the PRODH $\beta_8\alpha_8$ barrel domain as shown in Fig. 1B [19,51]. Unless a significant conformational change occurs during catalysis, there is not enough space for ubiquinone to bind at the *re*-face of the FAD. Our kinetic data and the observation that THFA does not disrupt DBMIB binding to PutA, indicates the *si*-face is also unlikely accessed by ubiquinone. Analysis of the THFA bound PRODH domain structure (PDB 1tiw) with CAVER found only two tunnels leading from the FAD cofactor using a cutoff radius of 1.4 Å [52,53]. The tunnels have highly conserved residues and are likely the entry points for proline leading to the binding site at the *si*-face of the FAD [19,54]. It is unlikely that ubiquinone could access these tunnels do to size constraints as the tunnels are narrow and have an average radii of 2.14 and 1.69 Å. Altogether, kinetic data and structural reasoning for PutA indicate that ubiquinone binds at a site distinct from that of proline. Thus, the location of the ubiquinone binding site remains an open question in PutA/PRODH biochemistry. From the structural analysis above, ubiquinone probably binds at a position distant from the FAD cofactor simply because of the lack of space available in the internal active site cavity (Fig. 1B). Spectral data from the FAD cofactor corroborates this hypothesis considering that no perturbation in the FAD spectrum was observed with CoQ_2 and DBMIB.

The effect of viscosity on the steady-state kinetic parameters was studied by varying proline in different fixed amounts of sucrose. Adding a viscosity agent is anticipated to only hinder diffusive steps in the mechanism, thus revealing if substrate binding or product release are rate limiting [41]. It was found that the viscosity effect on k_{cat}/K_m was negligible, while k_{cat} decreased 15–20% per unit viscosity. The lack of a strong viscosity effect on the kinetic parameters suggests that the overall reaction is not limited by diffusive steps, but most likely by a chemical step. The viscosity data also supports a rapid equilibrium assumption for the steady-state mechanism of PutA.

In summary, our steady-state kinetic data show a rapid equilibrium two-site ping pong mechanism for proline:ubiquinone oxidoreductase activity in PutA. Because sequence motifs in the PRODH catalytic core that are important for FAD and proline binding are shared among bacterial PutAs and eukaryotic PRODH enzymes, we predict that eukaryotic enzymes such as human PRODH will follow a similar kinetic mechanism found for *E. coli* PutA [1].

Acknowledgments

This research was supported by NIH GM061068 and is a contribution of the University of Nebraska Agricultural Research Division, supported in part by funds provided through the Hatch Act. This publication was also made possible by NIH Grant Number P20 RR-017675-02 from the National Center for Research Resources. Its contents are solely the responsibility of the authors and do not necessarily represent the official views of the NIH.

Appendix A. Supplementary data

Supplementary data associated with this article can be found, in the online version, at doi:10.1016/j.abb.2011.10.011.

References

[1] J.J. Tanner, Amino Acids 35 (2008) 719–730.
[2] J.L.A. Abrahamson, L.G. Baker, J.T. Stephenson, J.M. Wood, Eur. J. Biochem. 134 (1983) 77–82.

[3] D.H. Kohl, K.R. Schubert, M.B. Carter, C.H. Hagedorn, G. Shearer, Proc. Natl. Acad. Sci. USA 85 (1988) 2036–2040.
[4] J.M. Crawford, R. Kontnik, J. Clardy, Curr. Biol. 20 (2010) 69–74.
[5] K. Nagata, Y. Nagata, T. Sato, M.A. Fujino, K. Nakajima, T. Tamura, Microbiology 149 (2003) 2023–2030.
[6] B. Magasanik, C.A. Kaiser, Gene 290 (2002) 1–18.
[7] F. Bringaud, L. Riviere, V. Coustou, Mol. Biochem. Parasitol. 149 (2006) 1–9.
[8] J.W. Hargrove, J. Insect Physiol. 22 (1976) 309–313.
[9] L. Auerswald, P. Schneider, G. Gade, J. Exp. Biol. 201 (Pt 10) (1998) 1651–1657.
[10] L. Szabados, A. Savoure, Trends Plant Sci. 15 (2010) 89–97.
[11] C.H. Hagedorn, J.M. Phang, Arch. Biochem. Biophys. 248 (1986) 166–174.
[12] J.M. Phang, J. Pandhare, Y. Liu, J. Nutr. 138 (2008) 2008S–2015S.
[13] J. Curtis, G. Shearer, D.H. Kohl, Plant Physiol. 136 (2004) 3313–3318.
[14] K. Nakajima, S. Natsu, T. Mizote, Y. Nagata, K. Aoyania, Y. Fukuda, K. Nagata, Biomed. Res. (Tokyo) 29 (2008) 9–18.
[15] N. Krishnan, A.R. Doster, G.E. Duhamel, D.F. Becker, Infect. Immun. 76 (2008) 3037–3044.
[16] E. Brown, J.M. Wood, J. Biol. Chem. 267 (1992) 13086–13092.
[17] R. Menzel, J. Roth, J. Biol. Chem. 256 (1981) 9762–9766.
[18] M.W. Surber, S. Maloy, Biochim. Biophys. Acta 1421 (1999) 5–18.
[19] M. Zhang, T.A. White, J.P. Schuermann, B.A. Baban, D.F. Becker, J.J. Tanner, Biochemistry 43 (2004) 12539–12548.
[20] T.A. White, N. Krishnan, D.F. Becker, J.J. Tanner, J. Biol. Chem. 282 (2007) 14316–14327.
[21] D. Gu, Y. Zhou, V. Kallhoff, B. Baban, J.J. Tanner, D.F. Becker, J. Biol. Chem. 279 (2004) 31171–31176.
[22] Y. Zhou, J.D. Larson, C.A. Bottoms, E.C. Arturo, M.T. Henzl, J.L. Jenkins, J.C. Nix, D.F. Becker, J.J. Tanner, J. Mol. Biol. 381 (2008) 174–188.
[23] Y. Zhou, W. Zhu, P.S. Bellur, D. Rewinkel, D.F. Becker, Amino Acids 35 (2008) 711–718.
[24] E. Brown, J.M. Wood, J. Biol. Chem. 268 (1993) 8972–8979.
[25] J.M. Wood, Proc. Natl. Acad. Sci. USA 84 (1987) 373–377.
[26] W. Zhang, Y. Zhou, D.F. Becker, Biochemistry 43 (2004) 13165–13174.
[27] W. Zhang, M. Zhang, W. Zhu, Y. Zhou, S. Wanduragala, D. Rewinkel, J.J. Tanner, D.F. Becker, Biochemistry 46 (2007) 483–491.
[28] D. Srivastava, W. Zhu, W.H. Johnson Jr, C.P. Whitman, D.F. Becker, J.J. Tanner, Biochemistry 49 (2010) 560–569.
[29] S.B. Graham, J.T. Stephenson, J.M. Wood, J. Biol. Chem. 259 (1984) 2656–2661.
[30] I. Williams, L. Frank, Anal. Biochem. 64 (1975) 85–97.
[31] D.F. Becker, E.A. Thomas, Biochemistry 40 (2001) 4714–4722.
[32] I.H. Segel, Enzyme Kinetics Behavior and Analysis of Rapid Equilibrium and Steady-State Enzyme Systems, Wiley-Interscience, New York, 1975.
[33] A. Cornish-Bowden, Fundamentals of Enzyme Kinetics, third ed., Portland Press, London, 2004.
[34] J.S. Rieske, Methods Enzymol. 10 (1967) 239–245.
[35] Y. Nakashima, K. Shinzawa-Itoh, K. Watanabe, K. Naoki, N. Hano, S. Yoshikawa, J. Bioenerg. Biomembr. 34 (2002) 11–19.
[36] D.R. Lide, W.M. Haynes, CRC Handbook of Chemistry and Physics: A Ready-Reference Book of Chemical and Physical Data, 90th ed., CRC Press, Boca Raton, Florida, 2009.
[37] B.E. Eser, P.F. Fitzpatrick, Biochemistry 49 (2010) 645–652.
[38] J.R. Lakowicz, Principles of Fluorescence Spectroscopy, third ed., Springer, New York, 2006.
[39] R. Horsefield, V. Yankovskaya, G. Sexton, W. Whittingham, K. Shiomi, S. Omura, B. Byrne, G. Cecchini, S. Iwata, J. Biol. Chem. 281 (2006) 7309–7316.
[40] P.F. Cook, W.W. Cleland, Enzyme Kinetics and Mechanism, Garland Science, New York and London, 2007.
[41] H. Gutfreund, Kinetics for the Life Sciences: Receptors, Transmitters, and Catalysts, Cambridge University Press, Cambridge and New York, 1995.
[42] M. Simkovic, F.E. Frerman, Biochem. J. 378 (2004) 633–640.
[43] W. Zhu, Y. Gincherman, P. Docherty, C.D. Spilling, D.F. Becker, Arch. Biochem. Biophys. 408 (2002) 131–136.
[44] N.A. Malmquist, J. Baldwin, M.A. Phillips, J. Biol. Chem. 282 (2007) 12678–12686.
[45] K. Warncke, M.R. Gunner, B.S. Braun, L. Gu, C.A. Yu, J.M. Bruce, P.L. Dutton, Biochemistry 33 (1994) 7830–7841.
[46] D.B. Northrop, J. Biol. Chem. 244 (1969) 5808–5819.
[47] V. Hines, M. Johnston, Biochemistry 28 (1989) 1222–1226.
[48] F. Renosto, D.M. Ornitz, D. Peterson, I.H. Segel, J. Biol. Chem. 256 (1981) 8616–8625.
[49] M.P. Coughlan, K.V. Rajagopalan, Eur. J. Biochem. 105 (1980) 81–84.
[50] F. Forneris, A. Mattevi, Science 321 (2008) 213–216.
[51] Y.H. Lee, S. Nadaraia, D. Gu, D.F. Becker, J.J. Tanner, Nat. Struct. Biol. 10 (2003) 109–114.
[52] M. Petrek, M. Otyepka, P. Banas, P. Kosinova, J. Koca, J. Damborsky, J. BMC Bioinf. 7 (2006) 316.
[53] A. Pavelka, E. Chovancova, J. Damborsky, Nucleic Acids Res. 37 (2009) W376–W383.
[54] D. Srivastava, J.P. Schuermann, T.A. White, N. Krishnan, N. Sanyal, G.L. Hura, A. Tan, M.T. Henzl, D.F. Becker, J.J. Tanner, Proc. Natl. Acad. Sci. USA 107 (2010) 2878–2883.
[55] L.L.C. Schrodinger, The PyMOL Molecular Graphics System, Version 0.99, 2010.